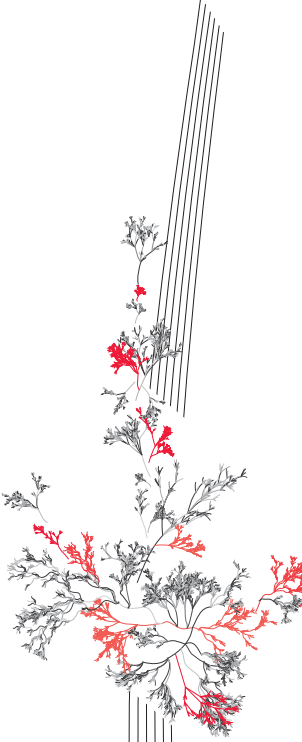
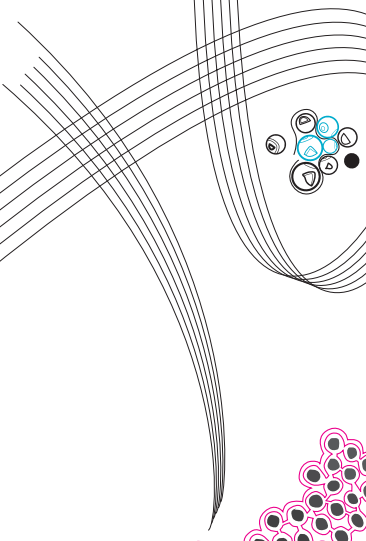
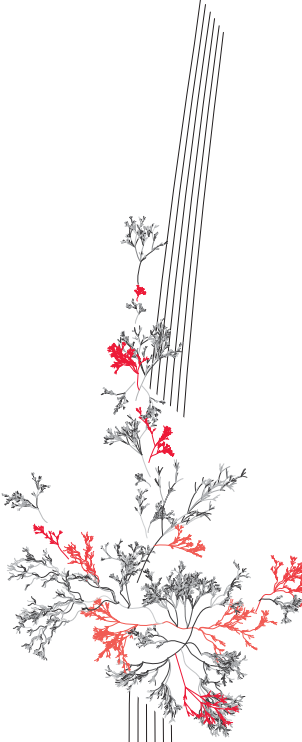


BSc Thesis Applied Physics & Applied
Mathematics

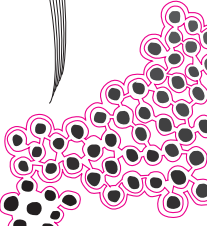
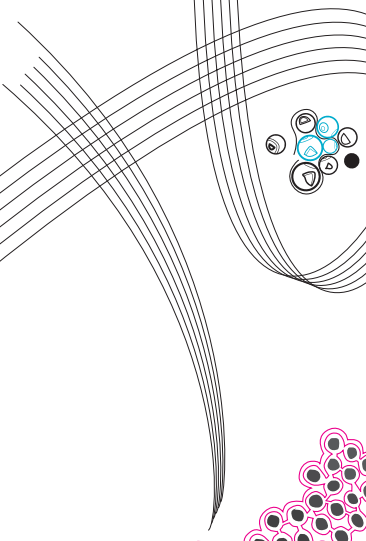
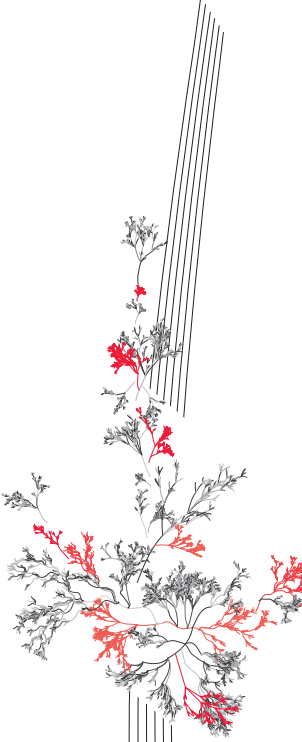


A semi-classical model for the thermoelectric properties of cubic SnSe

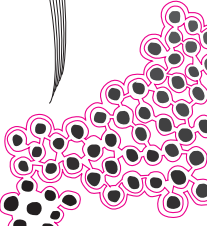
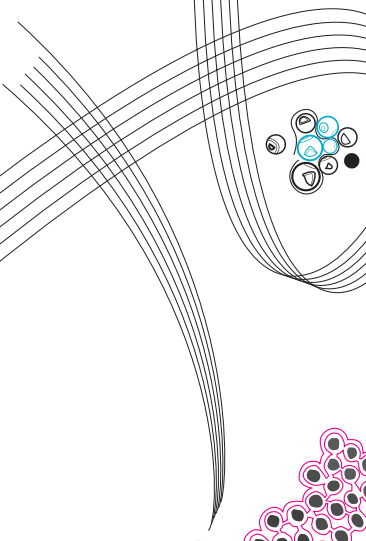
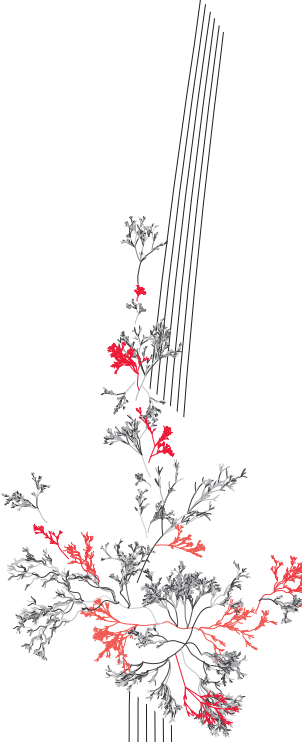


Geert Heres

Supervisors: Mark Huijben and Bernard Geurts



June 26, 2019



Department of Applied Mathematics
Faculty of Electrical Engineering,
Mathematics and Computer Science

A semi-classical model for the thermoelectric properties of cubic Tin Selenide

Geert Heres

June 26, 2019

Abstract

In this report two models for the thermoelectric effect were presented and applied to two materials. The first one focusses on using nano-structures to improve the thermoelectric properties of PbTe. It uses the relaxation time approximation for the dynamics of the electrons and quantum mechanics for the effects of the barriers. The second model uses a crude model of the density of states to calculate the thermoelectric properties of the cubic form of SnSe. It is found that the power factor has a local maximum for temperatures around 100K at a Fermi-energy just outside of the bandgap.

Keywords: thermoelectric effect, cubic SnSe, nano-structured PbTe

Contents

1	Introduction	3
1.1	Motivation	3
1.2	The effect	3
1.3	Important numbers	3
1.4	The goal	4
2	theory	5
2.1	Table of symbols	5
2.2	crystal structure	5
2.3	Density of states	6
2.4	Charge carrier concentration	6
2.5	Relaxation time approximation	8
2.6	Electron and holes	9
3	A model for PbTe	10
3.1	introduction	10
3.2	Density of states	10
3.3	Fermi energy	10
3.4	Relaxation times	11
4	Implementation of the model For PbTe.	15
4.1	Newton's method	15
4.2	Testing the model	16
4.3	Dependence on the barrier parameters	19
4.4	Constant relaxation time approximation	20
5	The model for (cubic) SnSe	22
5.1	Crystal structure	22
5.2	Density of states	22
5.3	Thermoelectric properties	25
5.4	Power factor	26
6	Conclusion	28
7	Outlook	28
8	Acknowledgements	28
	Bibliography	29

1 Introduction

1.1 Motivation

Due to the ever increasing demand for clean electricity, it is necessary to utilize the existing sources of clean energy more efficiently. One of the sources of energy that is not being used today is waste heat, which still contains a lot of energy. This energy can be converted into electricity using heat engines and generators. A problem of this approach is that heat engine often contain a lot of moving parts, which makes it impossible to implement them on most places. Thermoelectric materials are able to convert a temperature difference directly into electrical energy without any moving parts. Devices using this technology could be made very small and require barely any maintenance.

A problem of thermoelectric materials is that their efficiency is still very low. The search for new more efficient materials is a hot topic in the Inorganic material science (IMS) group. While most simple models mainly focus on PbTe, this group focusses on Tin Selenide (SnSe).

The difficulty in modelling the properties of SnSe lies in the crystal structure of the material. The normal form of SnSe has an orthorhombic structure, which has little symmetry. Recently it has been predicted that a cubic form of SnSe would have a very high thermoelectric efficiency at room temperature [5]. This prediction was made using a more complicated model that is partly based on density functional theory to calculate the electron distribution in the material. Due to the high symmetry of the cubic phase of SnSe it should be possible to calculate its properties using the semi-classical description of conduction.

1.2 The effect

When a material is heated on one side, electrons have a higher energy on average, which means that they will diffuse towards the cold side due to the concentration difference.. At the same time, low energy electrons will diffuse towards the hot side. If these currents are not equal, a nett current will flow from hot to cold until the electric force cancels out the diffusive force. This will create a voltage that can be measured experimentally. The relation between the temperature difference and the voltage is can be used to define the Seebeck coefficient according to $S = -\frac{\Delta V}{\Delta T}$. This coefficient has units of Volt per Kelvin. The minus sign makes it such that if the hot side gets a negative potential, then S is positive and vice versa. In general, the Seebeck coefficient is positive when the charge carriers are positive and it is negative when the carriers are negative. Interestingly, the units of S can also be interpreted as entropy per coulomb. So, the Seebeck coefficient describes how much entropy is created on average when the charge carriers move. This is also the way in which the classical expression for the Seebeck coefficient is determined from material properties.

1.3 Important numbers

A high Seebeck coefficient is not enough to guarantee that a material can efficiently generate electricity, Since the material can also conduct heat through its lattice without generating electricity. Also materials that do not conduct electricity very well are unlikely to have a high efficiency. The efficiency of a thermoelectric material is often given in the figure of merit, which is related to the absolute material. The figure of merit is defined as: $ZT = \frac{\sigma S^2 T}{\kappa}$, where κ is the thermal conductivity, σ is the electrical conductivity and S is the Seebeck coefficient.

The figure of merit is high in materials that have a high Seebeck coefficient and electrical conductivity and a low thermal conductivity. The reason that SnSe is a promising material is mainly due to its low thermal conductivity, which would give it a high efficiency.

Another important value is the thermoelectric power factor (P) defined as $P = \sigma S^2$. The power factor is a measure of the amount of electrical energy that can be produced by the material for a given temperature gradient. This is the property that can be optimized in the following models, because the thermal conductivity is not known accurately.

1.4 The goal

The goal of the research is to find out how to improve the power factor of semiconductor materials. Two material were considered; The first is nano-structured lead-telluride, which has been shown to have a very high thermoelectric efficiency [4]. The question is how the barriers should be tuned to get the optimal thermoelectric properties. Secondly, a new type of SnSe will be considered. For this material the goal is to find what the Fermi-energy should be to optimise the power factor.

2 theory

The Seebeck coefficient is given by the amount of entropy per coulomb that flows along with the temperature gradient. The entropy can be calculated as the flow of energy divided by the temperature. It is easiest to do this by first finding an expression for the number of electrons that flow and looking at the average energy gained at the cold end and due to the current.

In order to calculate the average energy in the electric current, it is necessary to find the flow of electrons as a function of their energy. Since the system as a whole is not in thermal equilibrium, the exact velocity distribution of the electrons cannot be calculated directly using the Fermi-Dirac distribution.

2.1 Table of symbols

Table I contains a list of symbols that are used for the physical constants in this report.

TABLE I: List of the symbols and values of the physical constants that are used in this report.

Symbol	Name	Value or unit
h	Planck's constant	$6.62607004 \cdot 10^{-34} \text{J s}$
\hbar	Reduced Planck's constant	$\frac{h}{2\pi} = 1,05457180 \cdot 10^{-34} \text{Js/rad}$
e	Elementary charge	$1.60217662 \cdot 10^{-19} \text{C}$
k_B	Boltzmann constant	$1,3806 \cdot 10^{-23} \text{J/K}$
ϵ_0	Permittivity of free space	$8.854188 \cdot 10^{-12} \text{F/m}$
m_0	Electron mass	$9.10938356 \cdot 10^{-31} \text{Kg}$

2.2 crystal structure

A crystal structure can be described as a combination of a Bravais lattice and its unit cell. A Bravais lattice consists of a set of position vectors as given in equation 1. Here \mathbf{a}_1 , \mathbf{a}_2 and \mathbf{a}_3 are the primitive lattice vectors. They determine the structure and periodicity of the lattice. The second important thing is the distribution of the atoms in the unit cell, this is called the basis of the crystal. The basis consists of the locations of the atoms in a unit cell expressed in the coordinates of the primitive vectors. Together these form the locations of all of the atoms in the crystal.

$$\mathbf{R} = \{n_1\mathbf{a}_1 + n_2\mathbf{a}_2 + n_3\mathbf{a}_3 | n_k \in \mathbb{Z}\} \quad (1)$$

Due to the wave-like nature of electron, it is often useful to look at the Fourier transform of the Bravais lattice. Since the real lattice is periodic in space, its Fourier transform consists of a series of Dirac delta functions. These peaks lie on a new lattice in the space of wavenumbers. This is also a Bravais lattice, which means that it can be described by a set of primitive vectors and linear combinations thereof.

In a crystal, the atoms create a periodic potential. due to this potential. The electron wavefunctions will form so-called Bloch waves, as described in equation 2. Here, $u(\mathbf{r})$ is a

periodic function with the same period as the crystal lattice, which depends on the exact shape of the potential created by the atoms. \mathbf{k} is called the wave-vector and has units of m^{-1} . It determines the direction in which the electron moves. For every possible \mathbf{k} , there exists a Bloch wave that solves the Schrödinger equation in the crystal. The energy of the waves depend on the shape of the function itself and it varies continuously with the wave-vector [17].

$$\psi(\mathbf{r}) = e^{i\mathbf{k}\cdot\mathbf{r}}u(\mathbf{r}) \tag{2}$$

The relation between the wave-vector and the corresponding energy is called the dispersion relation. The states with wave-vectors that differ by a reciprocal lattice vector are equivalent in the sense that their corresponding Bloch waves are the same. This equivalence makes it possible to describe all unique electron states by looking at a single reciprocal unit cell. This unit cell is called the Brillouin zone and contains all the information that is necessary in the following models. Hence, all relevant information is included in the dispersion relation of the Brillouin zone.

2.3 Density of states

Most macroscopic electronic properties of a material depend on the energy distribution of the conducting electrons. This distribution can be split into two parts; The density of states (DOS), which gives the number of possible states with a certain energy, and the occupation of those states.

The density of states is given by the number of states per unit volume per unit of energy. This means that when integrated over the energy, it becomes a concentration. It can be calculated by counting how many states fall within a small energy interval and then dividing by the length of the interval. In general, it is difficult to find a good approximation of the density of states.

2.4 Charge carrier concentration

In a semiconductor at zero temperature, all the states below the band gap are filled with electrons. In that case, the momentum of an electron can only change, if it is excited to the conduction band. In that band it can gain momentum from an electric field and contribute to conduction.

When an electron is excited to the conduction band, it leaves a positively charge vacancy in the crystal, often called a hole. This hole can move around in the crystal in the same way as an electron. Allowing it to be described like a free positive particle.

As the temperature increases, the thermal energy of the particles will go up. This allows some of the electron to get excited to the conduction band. This process can be described using quantum statistical mechanics. The occupancy of a state is given by the Fermi-Dirac distribution (equation 3) depends on the difference of its energy and the chemical potential, in units of the thermal energy $k_B T$. The scaling with the thermal energy results in broadening of the function as the temperature increases. In figure 1 the function is plotted for a number of

temperatures, all graphs use the same Fermi-energy.

$$f(E) = \frac{1}{1 + e^{(E-\mu)/k_B T}} \quad (3)$$

The holes are distributed according to the complement of this distribution, which can be rewritten according to equation 4.

$$f_h(E) = 1 - f(E) = 1 - \frac{1}{1 + e^{(E-\mu)/k_B T}} = \frac{e^{(E-\mu)/k_B T}}{1 + e^{(E-\mu)/k_B T}} = \frac{1}{1 + e^{-(E-\mu)/k_B T}} \quad (4)$$

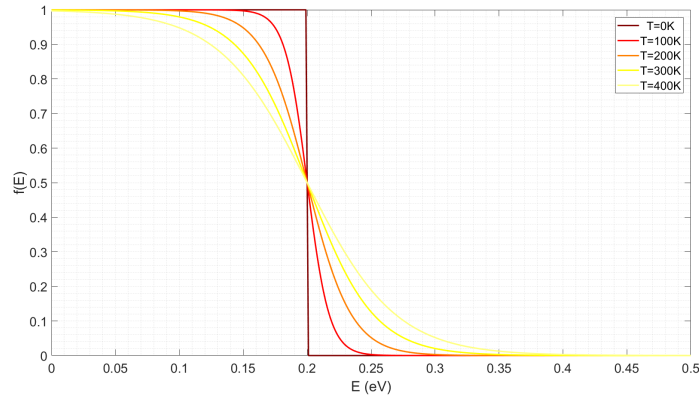


FIGURE 1: The Fermi-Dirac function at different temperatures. The Fermi energy is kept at 0.2 eV.

The total number of electrons with a certain energy is given by the product of the density of states and the occupancy. The total number of carriers can be found by integrating this over all relevant energies. For electrons that is the region above the Fermi energy, and for the holes it is the region below. If the Fermi energy lies in the band gap, then the charge carrier concentration can be calculated using equations 5 and 6.

$$n_0 = \int_{E_c}^{\infty} DOS(E) \frac{1}{1 + e^{(E-E_f)/k_B T}} dE \quad (5)$$

$$p_0 = \int_{-\infty}^{E_v} DOS(E) \frac{1}{1 + e^{-(E-E_f)/k_B T}} dE \quad (6)$$

Conservation of charge states that these two concentrations must be equal, which is stated in equation. This equality can be used to determine the Fermi energy given the density of states. Due to the broadening of the Fermi-Dirac function, the concentration of both will increase with temperature. The increase in concentration causes the conductivity of semiconductors to increase as well.

Another way to increase the carrier concentration is by adding dopant atoms. These atoms will settle in the crystal and will accept or donate electron. If the dopants take electron from the material then it is called p-type doping. p for positive, because the created holes are positive. If the dopant donates an electron, then it is called n-type doping.

When a dopant is used, the electron concentration can be different from the hole concentration. The dopant atoms will be left with a stationary charge and they can act as scattering potentials. Thus if an electron donor were added to the material with binding energy E_D and concentration N_D , then that would result in $n_D = f_h(E_D) \cdot N_D$ additional conducting electrons and an equal amount of stationary positive charges. The Fermi-energy can then still be calculated using charge conservation[16].

$$p_0 + N_D^+ = n_0 + n_D$$

$$\int_{-\infty}^{E_v} DOS(E) f_h(E) dE + f_h(E_D) N_D = \int_{E_c}^{\infty} DOS(E) f(E) dE \quad (7)$$

From equation 7 it is clear that the Fermi-energy has to increase when the dopant concentration increases, this means that it is possible to adjust the position of the Fermi-energy using appropriate amounts of doping. It is also possible to lower the Fermi-energy by adding electron acceptors instead. The final concentration and the position of the Fermi-energy depend on the shape of the density of states as well as on the temperature.

2.5 Relaxation time approximation

The most commonly used way to estimate the electron distribution is the so called relaxation time approximation [6],[2]. In this model the electrons are assumed to be distributed according to some non-equilibrium distribution function. When the system is in thermal equilibrium the function has to be equal to the Fermi-Dirac function, which is shown in 3.

The relaxation time approximation is based on two central assumption. The first is that the distribution of the electrons after a collision is independent of the distribution prior to the collision and the is that the collisions do not change the distribution if they already follow the equilibrium distribution. Collision are assumed to on average occur once per relaxation time τ . In generals, this relaxation time can depend on both the momentum of the carriers. However, in an isotropic material the momentum dependence is often assumed to occur only through the energy of the carrier. This is a good approximation in most isotropic material and it simplifies all further calculation.

Then three assumption need to be made in order to get the desired results. firstly, Both the temperature and potential gradients are assumed to be weak. This ensures that currents can be considered to be linear in the electric field. Also heat transport is linear in the temperature gradient and the electrical current. A consequence of this is that Coulomb heating due to resistance is neglected, because it scales with the square of the current. Secondly, the temperature gradient is taken to be constant over the material. This is true if the system has reached a thermal steady state, this also implies that the heat flow is constant in time. Lastly, the material is considered to be homogenous, so it has the same properties everywhere.

In general crystals, the conductivity can depend on the direction of the current. If the crystal has cubic symmetry then the conductivity is the same in each direction. PbTe and cubic SnSe both have this symmetry. Finally, the resulting expression for the conductivity is given in equation 8.

$$\sigma = \frac{2e^2}{3m^*} \int_0^\infty \tau(E)DOS(E)E \left(-\frac{\partial f(E)}{\partial E} \right) dE \quad (8)$$

Then, the average energy in the induced current can be calculated using equation 9. The second equality follows from the fact that the current is proportional to the conductivity.

$$\bar{\epsilon} = \frac{\int_0^\infty \epsilon j(\epsilon) d\epsilon}{\int_0^\infty j(\epsilon) d\epsilon} = \frac{\int_0^\infty \tau(E)DOS(E)E^2 \left(-\frac{\partial f(E)}{\partial E} \right) dE}{\int_0^\infty \tau(E)DOS(E)E \left(-\frac{\partial f(E)}{\partial E} \right) dE} \quad (9)$$

Then, the relation between energy flow and entropy can be used to determine the flow of energy per charge carrier. since the carriers at the cold end already have energy, it is necessary to subtract the average of that energy from the average incoming energy. The average energy of carriers is given by the chemical potential μ . Then a factor of $\frac{1}{e}$ is needed to convert this to entropy per coulomb. Finally, the expression for $\bar{\epsilon}$ can be substituted in the equation to obtain the final results in equation 10. From this equation it can be seen that the Seebeck coefficient is largest if the scattering time increases with the energy.

$$S = \frac{1}{e} \left(\frac{\bar{\epsilon}}{T} - \frac{\mu}{T} \right) = \frac{1}{eT} \left[\frac{\int_0^\infty \tau(E)DOS(E)E^2 \left(-\frac{\partial f(E)}{\partial E} \right) dE}{\int_0^\infty \tau(E)DOS(E)E \left(-\frac{\partial f(E)}{\partial E} \right) dE} - \mu \right] \quad (10)$$

The derivative of the Fermi-Dirac function: $-\frac{\partial f(E)}{\partial E}$ is a peaked function around the Fermi energy with a width of about $5k_B T$. As the temperature decreases, $-\frac{\partial f(E)}{\partial E}$ will get a sharper and higher peak. The Fermi-Dirac function goes precisely from 1 to 0, So the integral of this function is always equal to 1. This means that the function converges to the Dirac delta function as the temperature goes to zero.

2.6 Electron and holes

when both electrons and holes contribute to the charge transport, they will generate an opposing thermoelectric voltage (The Seebeck coefficients have different signs). The total Seebeck coefficient is the average off the separate coefficients, weighted by their corresponding conductivity. This is explicitly described in equation 11, where the subscript denotes the type of carrier responsible for the effect [6].

$$S = \frac{\sigma_e S_e + \sigma_h S_h}{\sigma_e + \sigma_h} \quad (11)$$

3 A model for PbTe

3.1 introduction

In 2009, Popescu et al. created a model for the thermoelectric properties of lead telluride (PbTe) based on the relaxation time approach. They assumed that the relaxation times of the charge carriers only depends on their energy and the overall temperature, meaning that they neglected any directional effects. The question of this specific article is how to model a material consisting of grains instead of a single piece of material. Such a nanocomposite material contains a lot of grain boundaries, which serve as scattering sites for the charge carriers. The boundaries will decrease the mobility of low energy carriers more than that of the high energy carriers. This will increase the average energy per charge carrier, which in turn increases the Seebeck coefficient. they use the two- state Kane model to approximate the density of states of PbTe. The material mostly consists of normal PbTe, so, they neglect the effects that the grain boundaries have on the electronic properties. They choose to fix the charge carrier concentration and use it to calculate the Fermi energy, while assuming that the system is in thermal equilibrium. Finally, they use expressions for the intrinsic scattering times found in literature.

3.2 Density of states

Tin Selenide is a material with a small bandgap. The band structure is slightly non-parabolic. It is possible to model the band structure of small bandgap thermoelectric materials using the so called two-band Kane model[10]. This model assumes that the dispersion relation of the carriers is non parabolic. In most small bandgap semiconductors (including PbTe) the nonparabolicity can be approximated in terms of the bandgap in a simple way. This results in the density of state shown in equation 12. The equation contains the effective mass m^* , which is a material dependent physical parameter that can be measured independently. The effective mass has been independently found at $0.16m_0$, where m_0 is the mass of an electron.

$$DOS(E) = \frac{\sqrt{2}}{\pi^2} \left(\frac{m^*}{\hbar^2} \right)^{3/2} \sqrt{E(1 + E/E_g)(1 + 2E/E_g)} \quad (12)$$

3.3 Fermi energy

The Fermi energy, also called chemical potential is very important in this model, since it determines the location of the strongly peaked function. As stated before, the researchers have decided to calculate the Fermi energy from the charge carrier density. This is an unconventional way to model semiconductors, because the charge carrier density in a material depends strongly on the temperature and changing keeping the charge carrier density constant over a range of temperatures is not possible in a single sample of a semiconductor. To keep the concentration constant, multiple samples would have to be made, each having a different concentration of dopant atoms. Most other models either use the dopant concentration as an input or they treat the Fermi energy as the controllable parameter, and they use that to calculate the carrier concentration given the dopant concentration and temperature. Both methods have the advantage that they also give the concentration of ionized dopant atoms, which is needed to calculate the impurity scattering time. In this model the impurity concentration is fixed at 15% of the charge carrier concentration. In [13], the charge carrier concentration in PbTe was

found to be given by equation 13. In this equation, ν is the degeneracy of the contributing energy levels. For PbTe, $\nu = 4$.

$$N = \frac{4\nu}{\sqrt{\pi}} \left(\frac{2\pi m_{dn}}{h^2} \right)^{3/2} \left(F_{1/2}(\eta) + \frac{2kT}{E_g} F_{3/2}(\eta) \right) \equiv K \left(F_{1/2}(\eta) + \frac{2kT}{E_g} F_{3/2}(\eta) \right) \quad (13)$$

Where,

$$F_i(\eta) = \int_0^\infty x^i f_0 dx$$

$$x = \frac{E}{k_B T}, \quad f_0 = \frac{1}{e^{x-\eta} + 1}, \quad \text{and } \eta = \frac{\mu}{kT}$$

This results in a problem, because of the dimensionality of the system. The integral is already non-dimensional, so the only term with units is the factor K in front of the integral. Since everything is done in SI-units, it is possible to rewrite the units of m^* into $\frac{Js^2}{m^2}$. The unit of for Planck's constant is $J \cdot s$. Combining these gives for the units of K:

$$[K] = \left(\frac{kg}{J^2 s^2} \right)^{3/2} = \left(\frac{Js^2}{m^2 J^2 s^2} \right)^{3/2} = \left(\frac{1}{m^2 J} \right)^{3/2} = m^{-3} J^{-3/2}$$

This means that the result is not a concentration. An additional factor of $(k_B T)^{3/2}$ in the pre-factor would fix this problem. This is also exactly the term that comes from the substitution to the dimensionless energy. Including that into the expression results in equation 14, which is te one that will be used in the following sections.

$$p = \frac{4}{\sqrt{\pi}} \left(\frac{2\pi m^*}{h^2} \right)^{3/2} \int_0^\infty E^{1/2} f(E) dE \equiv C_\mu \int_0^\infty E^{1/2} f(E) dE \quad (14)$$

3.4 Relaxation times

The relaxation time can be split into four parts that can be added according to equation 15. The total relaxation time will be smaller than any of the separate relaxation times. This means that it is possible for one of the scattering effects to dominate over the others.

$$\frac{1}{\tau(E)} = \sum_i \frac{1}{\tau_i(E)} \quad (15)$$

In most semiconductors, the scattering times have theoretically been found to depend on the energy in the following way $\tau(E) = a_s E^s$, where a is a material parameter that may depend on temperature. [3].

where $s = -\frac{1}{2}$ for acoustic phonon scattering, $\frac{1}{2}$ for optical phonons and $\frac{3}{2}$ for impurities.

Where the pre-factors are given by the equations below.

$$a_{-\frac{1}{2}} = \frac{h^4 \rho v_L^2}{8\pi^3 k_B T} \frac{1}{(2m^*)^{3/2} D^2}$$

$$a_{\frac{1}{2}} = \frac{h^2}{2^{1/2} m^{*1/2} e^2 k_B T (\varepsilon_\infty^{-1} - \varepsilon_0^{-1})}$$

$$a_{\frac{3}{2}} = \left[\frac{Z^2 e^4 N_i}{16\pi (2m^*)^{1/2} \varepsilon^2} \ln \left[1 + \left(\frac{2E}{E_m} \right)^2 \right] \right]^{-1}$$

These formulas contain several material parameters, most of which can be determined from other experiments. The names and values of the parameters are given in table II. The last parameter needs some attention, since it contains the

TABLE II: Names and values of the parameters used in the expressions for the relaxation times.

Symbol	Parameter	Value	Source
ρ	mass density	8160	[10]
m^*	effective mass	$0.16m_0$	[10]
v_L^2	Speed of sound	1730m/s	[10]
D	Deformation potential	7eV	Determined from fit
$(\varepsilon_\infty^{-1} - \varepsilon_0^{-1})$	Related to dielectric constant	$.0072E_g(eV)$	[10]
ε	Dielectric constant	$26.3\varepsilon_0$	[8]
N_i	Impurity concentration	0.15p	[10]
Z	Impurity charge	1	[10]
E_m	Mean attraction energy from impurity	$E_m = \frac{Ze^2}{4\pi\varepsilon r_m}$	[10]
r_m	Mean distance to an impurity	$\frac{1}{2N_i^{1/3}}$	[10]

Then they also consider the scattering from a grain boundary. They model the grain boundaries as rectangular potential wall with a constant height and width. It is assumed that the distance between the walls is constant. A schematic view of such barriers is shown in figure 2. It is possible to analytically calculate the transmission probability of such a barrier for electrons using quantum mechanics.

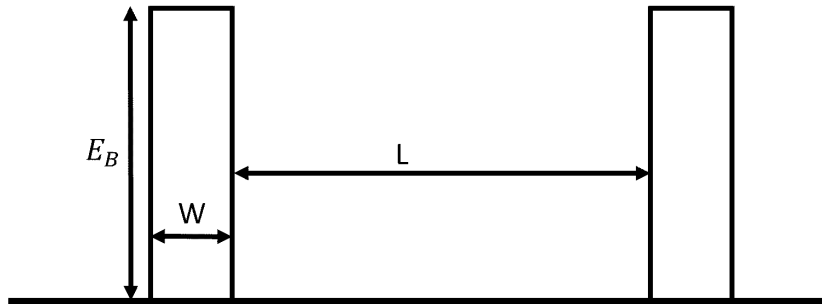


FIGURE 2: A schematic representation of the barriers used in the model

It is assumed that all scattering events are independent, which is true if the barriers are far apart, or if other scattering events take place, since then all phase information of the electron wave is lost. This assumption means that only the amplitude of the scattered wave is important. This transmission amplitude is given in equation 16. It follows directly from the continuity of the electron wave function and its derivative [15].

$$T = |t|^2 = \left[1 + \frac{E_B^2 \sinh^2(k_1 L)}{4E(E_B - E)} \right]^{-1} \quad (16)$$

$$k_1 = \sqrt{\frac{2m^* E_b w^2}{\hbar^2} \left(1 - \frac{E}{E_b} \right)}$$

The mean free path length can be determined by assuming the transmission to be equal for all the barriers. The number of barriers that the electron travels through then follows a geometrical distribution with success probability (1-T). The expected distance can then be expressed as in equation 17. The upper limit is taken to go to infinity to make it possible to calculate analytically. This is allowed, because real materials are a lot larger than the distance between the barriers, so the electrons can be scattered a very large amount of times.

$$\begin{aligned} \lambda &= \sum_{n=0}^{N \rightarrow \infty} T^n (1-T) n L = (1-T) L \sum_{n=0}^{N \rightarrow \infty} T \frac{dT^n}{dT} = T(1-T) L \frac{d}{dT} \sum_{n=0}^{N \rightarrow \infty} T^n \\ &= T(1-T) L \frac{d}{dT} \frac{T}{1-T} = T(1-T) L \frac{d}{dT} \frac{1}{1-T} = T(1-T) L \frac{1}{(1-T)^2} = \frac{TL}{1-T} \end{aligned} \quad (17)$$

Then the expression of T can be substituted in 17. This is shown in equation 18. an additional L/2 is added to the mean free path, because the electron will on average be a distance of L/2 away from the first barrier. In the last step the definition of k_1 was used.

$$\begin{aligned} \lambda &= L \left(\frac{1}{2} + \frac{T}{1-T} \right) = L \left(\frac{1}{2} + \frac{1}{\frac{1}{T} - 1} \right) \\ &= L \left(\frac{1}{2} + \frac{1}{1 + \frac{E_B^2 \sinh^2(k_1 a)}{4E(E_B - E)} - 1} \right) = L \left(\frac{1}{2} + \frac{4 \frac{E}{E_b} \left(1 - \frac{E}{E_b} \right)}{\sinh^2 \left[\sqrt{\frac{2m^* E_b w^2}{\hbar^2} \left(1 - \frac{E}{E_b} \right)} \right]} \right) \end{aligned} \quad (18)$$

The scattering time due to these barriers is calculated as the mean free path length divided by the velocity of the carriers. The velocity can be approximated by $\sqrt{\frac{2E}{m^*}}$. Since k_1 is a complex number when $E > E_B$, the hyperbolic sine can be replaced by minus one times sine of the absolute value of k_1 . This results in the two cases for the relaxation time that are shown in 19.

$$\tau_b(E) = \begin{cases} L\sqrt{\frac{m^*}{2E}} \left[\frac{1}{2} + \frac{4\frac{E}{E_b}\left(1-\frac{E}{E_b}\right)}{\sinh^2\left(\sqrt{\frac{2m^*E_b w^2}{\hbar^2}\left(1-\frac{E}{E_b}\right)}\right)} \right] & E < E_b \\ L\sqrt{\frac{m^*}{2E}} \left[\frac{1}{2} + \frac{4\frac{E}{E_b}\left(\frac{E}{E_b}-1\right)}{\sin^2\left(\sqrt{\frac{2m^*E_b w^2}{\hbar^2}\left(\frac{E}{E_b}-1\right)}\right)} \right] & E > E_b \end{cases} \quad (19)$$

In [9], a sample of nanostructure PbTe was made. They fitted a similar model to their data and found the following parameters: $W \approx 50nm$, $L \approx 300nm$ and $E_B \approx 60meV$. These values will be used in this following section.

4 Implementation of the model For PbTe.

it is relatively straightforward to implement the model as described before. It is important to make sure that the units that are used are all consistent with each-other, since some the energies are given in eV. Which means that there will be a lot of conversion factors. It is easier to avoid any confusion by just using SI units for every formula. Then there is no risk of missing conversion factors.

The model so far has been derived in continuous energy space, so the first step will be to choose an energy grid for the integration. All relevant integrals contain either the Fermi-Dirac function or its derivative. Both of them decrease exponentially. In [13] it was calculated that the Fermi energy will be smaller than (0.07 eV) over the whole temperature range. The highest temperature that is used is 300K at which point the thermal energy is $k_B * 300 \approx 0.026eV$.

The Fermi-Dirac function reduces to the order of 10^{-5} when the difference between the energy and the Fermi energy is 10 times the thermal energy. Its derivative is proportional to the function itself, so it will also be very small at that point. At 300K, this results in an energy of 0.33eV, which should be sufficient as an upper bound for the energy grid. The step size should also be small enough to give accurate results. Here a step size of 0.1meV was used. This gives a total number of grid point in the order of 1000, which seems to be sufficient. This will be checked later.

4.1 Newton's method

One thing that deserves attention is the determination of the Fermi-energy. Since the integral equation does not have a simple it is easiest to use a root finding algorithm to find the Fermi energy. The task is to find a value of ν such that equation 14 holds. This can be rewritten into equation 20.

$$\int_0^{\infty} E^{1/2} f(E, \mu) dE - \frac{p}{C_{\mu}} = g(\mu) = 0 \quad (20)$$

Now, $g(\mu)$ is strictly increasing, which can be shown from its derivative, this is done in equation 21, the final step uses integration by parts and the fact that the Fermi-Dirac distribution decays exponentially for large energies. Both factors of the integrand are positive for $E > 0$. This means that there can be at most one solution to equation 20.

$$g'(\mu) = \frac{\partial}{\partial \mu} \left[\int_0^{\infty} E^{1/2} f(E, \mu) dE - \frac{p}{C_{\mu}} \right] = \int_0^{\infty} E^{1/2} \frac{\partial f(E, \mu)}{\partial \mu} dE = 1/2 \int_0^{\infty} E^{-1/2} f(E, \mu) dE \quad (21)$$

There are multiple ways to solve this root finding problem, but here Newtons method will be used. Newton's method is an iterative process that converges towards the root of the function. at any step μ_n , a better guess for the root is given by equation 22[14]. If it converges, this process can be repeated until the value of the function is arbitrarily small. In this case the

algorithm stops when $g(\mu) < 10^{-9}$, which often takes four or five iterations, dependent on temperature and carrier concentration.

$$\mu_{n+1} = \mu_n - \frac{g(\mu)}{g'(\mu)} \quad (22)$$

Because $E^{-1/2}$ diverges at zero energy, it is better to use the second to last expression of equation 21 for the numerical implementation of Newton's method. In figure 3 the convergence of the estimate to the correct value is shown. The black line is the function $g(\mu)$, and the red dots are the points that were needed for Newton's algorithm. From this graph it appears to work as intended, the final value of $g(\mu)$ is $2.6 * 10^{-18}$, which further confirms this. .

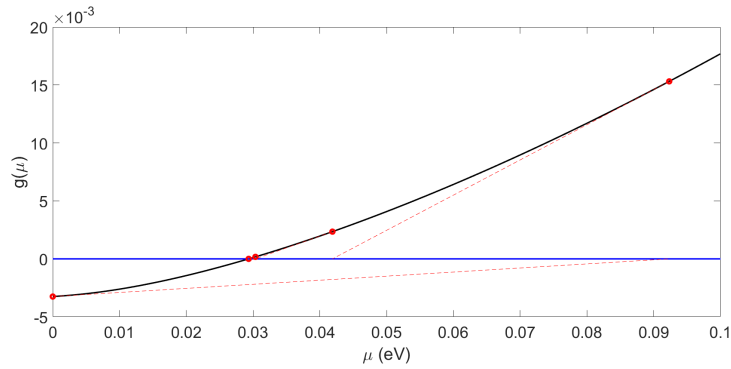


FIGURE 3: The convergence of the Fermi-energy using Newton's method, starting from $E=0$.

4.2 Testing the model

The authors of the paper used data of a sample that had no ionized impurities to calibrate their model. The data they used can be seen in the left figure 4. Then this model was used to get the results of the right figure. The calculated conductivity is reasonably close to the results from the article, but the Seebeck coefficient has a different shape. The value of the Seebeck coefficient is close at high and low temperatures. In between the calculated graph has a different shape than the one from the article. It is not clear why that is the case. It was not possible to change the parameters such that the Seebeck coefficient had about the correct shape, without disturbing the conductivity too much. The conductivity increases with the carrier density, which is to be expected. The Seebeck coefficient does the same at low temperatures and it does the opposite at higher temperatures. This is visible in both the results from the article and the calculations.

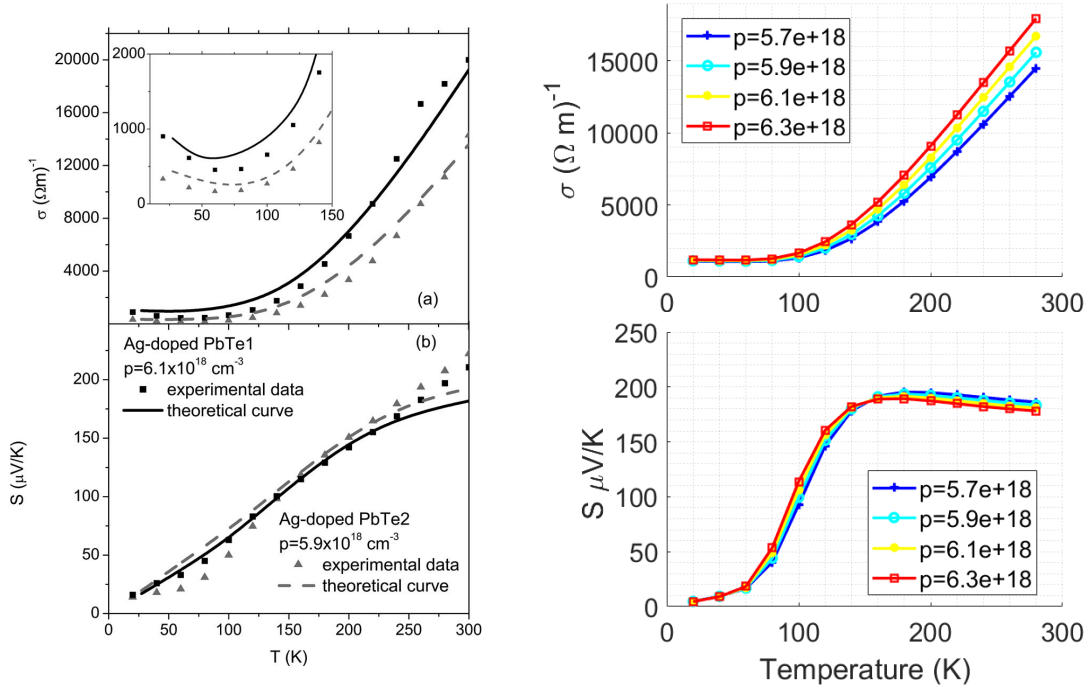


FIGURE 4: The conductivity and the Seebeck coefficient as a function of temperature for different carrier concentrations without taking the impurity scattering into account. The left graph shows the results from [10], and the right graph shows the results from the model above.

Then the impurity scattering time was added into the model. the resulting graphs are shown in figure 5. The new conductivity is about ten times smaller than before, but it still increases with temperature and the carrier concentration. The Seebeck coefficient has changed qualitatively in the sense that it decreases with carrier concentrations for all temperatures. Its value has increased as well.

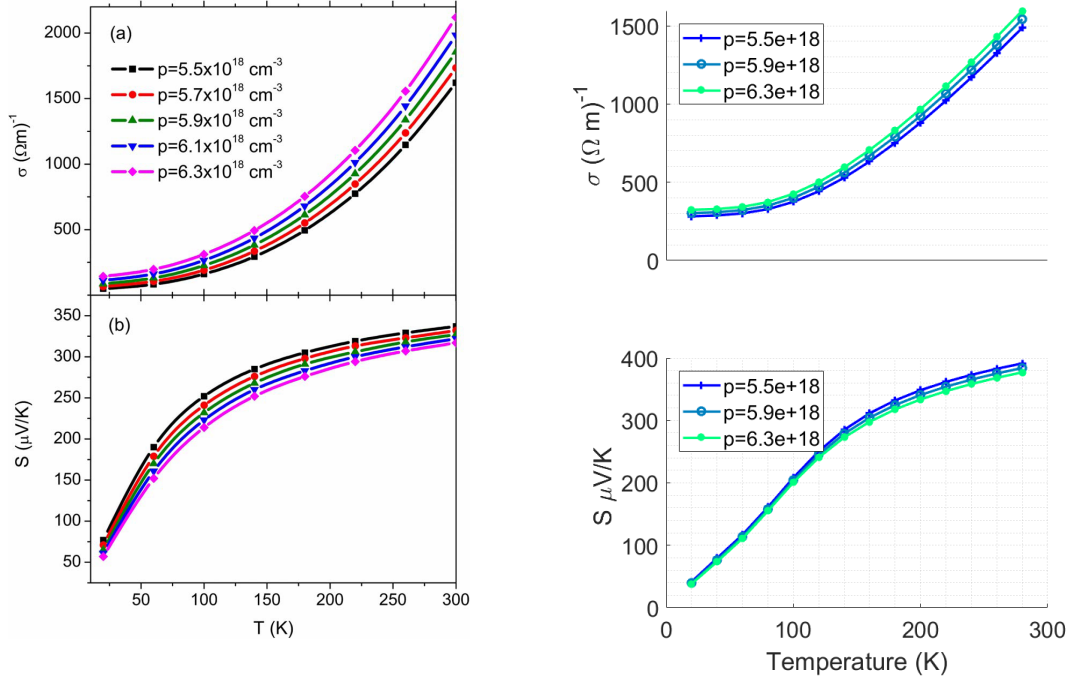


FIGURE 5: The conductivity and the Seebeck coefficient as a function of temperature for different carrier concentrations. The left graph shows the results from [10], and the right graph shows the results from the model above.

Checking the energy step size

The model was run with different energy steps. The results are shown in table III. The full calculation was done at the highest and the lowest temperature to see whether the temperature needs to be considered when choosing the energy grid. The carrier concentration is set to $5.9 \cdot 10^{18} \text{ cm}^{-3}$. The error is the difference between that calculation and the most accurate one as a percentage of the latter. The error decreases with the step size. The relative error changes less than 0.02% at both temperatures when the step size is decreased further than 0.1meV. This is small enough to not really be noticeable, which means that the initial guess for the step size can be used for all temperatures in the region of interest

TABLE III: The Seebeck coefficient calculated using different energy step sizes. At 50K (left) and 300K (right).

ΔE (meV)	$S(\mu V/K)$	error (%)	ΔE (meV)	$S(\mu V/K)$	error (%)
10	59.2	-8.4	10	352.6	$-6.5 \cdot 10^{-1}$
1	64.630	$-2.2 \cdot 10^{-2}$	1	354.2	$-2.0 \cdot 10^{-2}$
0.1	64.639	$-8.6 \cdot 10^{-3}$	0.1	354.897	$-2.6 \cdot 10^{-3}$
0.01	64.6442	$-2.6 \cdot 10^{-4}$	0.01	354.9057	$-8.7 \cdot 10^{-5}$
0.001	64.644327	$-8.1 \cdot 10^{-6}$	0.001	354.90604	$-2.7 \cdot 10^{-6}$
0.0001	64.644333	0 (definition)	0.0001	354.90603	0 (definition)

4.3 Dependence on the barrier parameters

It is interesting to see how the thermoelectric properties depend on the parameters of the potential barriers. In figure 6 the conductivity and Seebeck coefficient are plotted as a function of the barrier height. As expected, the conductivity decreases as the barrier height increases. The behaviour of the system is the same for the different carrier concentrations. At room temperature, the Seebeck coefficient increases with the barrier height, as shown in figure 6b. This is due to the filtering of the low-energy charge carriers. This increases the average energy per carrier and thus the Seebeck coefficient. At lower temperatures the increase stops at a certain height (figure 6a). This is probably due to the narrower derivative of the Fermi function, since the filtering is only effective when there are many carriers with higher energy than the barrier. When the barrier is significantly higher than the Fermi-level, the filtering no longer works to increase the Seebeck coefficient. This is further supported by the fact that the optimal barrier height increases with the carrier concentration and thus the Fermi-energy.

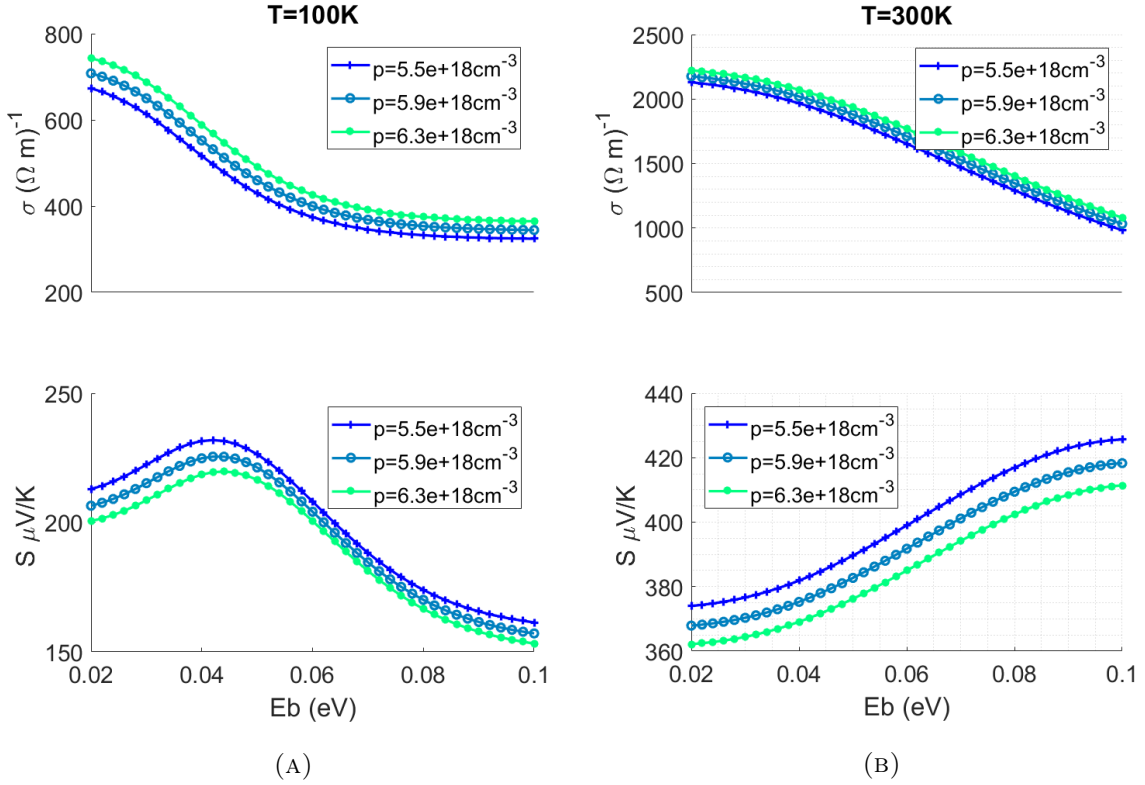


FIGURE 6: The conductivity and Seebeck coefficient as a function of the barrier height. The temperature is set to 100K and 300K for the left and right figures respectively, all other parameters are the same as before.

In figure 7 the power factor is shown as a function of the barrier height. at 300K temperatures the power factor is higher for lower barrier heights. At 100K a maximum is visible around 30meV. This shows that these energy barriers can be used to increase the power factor of PbTe. The optimal concentration also depends on the barrier height. When the barriers are low, it is better to have a low carrier concentration, while for higher barriers it is better to have

more carriers. Important to note is that the article in [10] reports a power factor at 300K that is about 1.5 times smaller than the one presented here. This is due to their lower Seebeck coefficient at high temperatures.

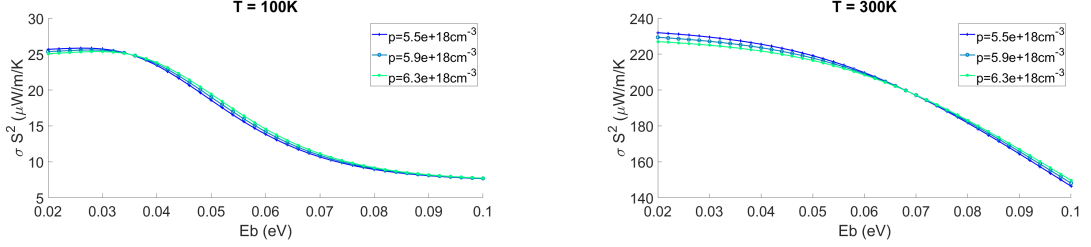


FIGURE 7: The power factor as a function of the barrier height. The temperature is 100K and 300K for the left and right figures respectively, all other parameters are the same as before.

4.4 Constant relaxation time approximation

Since determining the relaxation time of the carrier in a material is very difficult in general due to the large number of parameters involved, it is often assumed to be constant. Then it is either set to a typical value, often ($10^{-14}s$), or it is divided out of the quantities that have time in their unit. The unit of conductance then becomes $\frac{1}{\Omega ms}$. To find the actual conductance it must be multiplied by the relaxation time. A consequence of this is that the reported values will be fourteen orders of magnitude higher than normal. The Seebeck coefficient does not have time in one of its units, so its units will not change.

Removing the energy dependence of the relaxation time has a large influence on the temperature dependence of the quantities, not only because of the temperature dependence, but also because the Fermi-window shifts as the temperature changes. To get a better look at the implications of the constant relaxation times, the Seebeck coefficient and conductivity have been calculated in this approximation. The results are shown in figure 8.

Clearly the graphs are a lot flatter and the Seebeck coefficient is smaller over the whole range. The trends that were present before are still there; the conductivity increases with temperature and carrier concentration, while the Seebeck coefficient increases with temperature, but decreases with carrier concentration. This shows that is approximation can be used to determine trends, but not to get good quantitative answers.

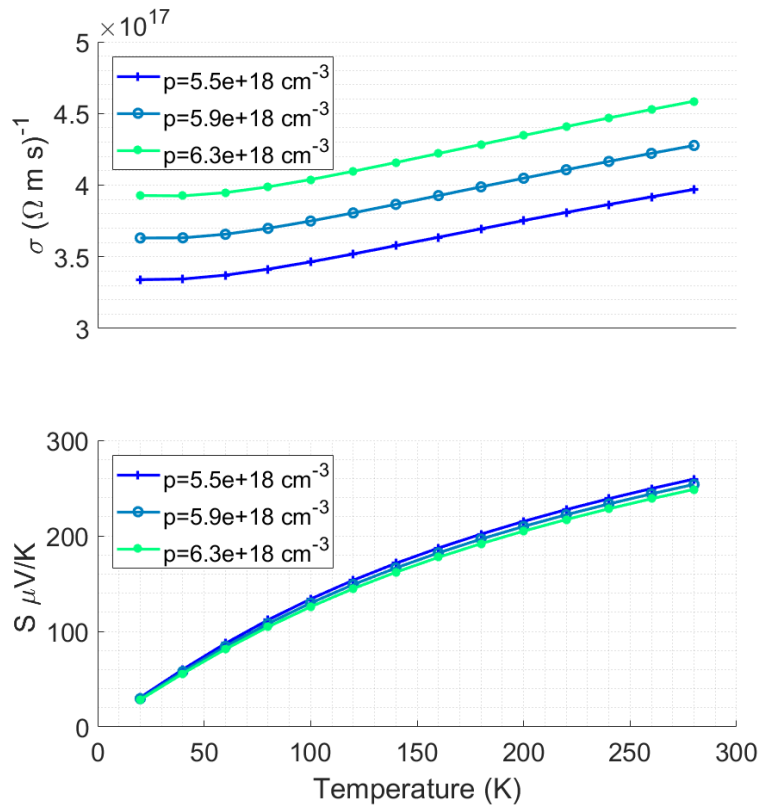


FIGURE 8: The Seebeck coefficient and electrical conductivity calculated with respect to the relaxation time

5 The model for (cubic) SnSe

5.1 Crystal structure

The common form of Tin-selenide (α -SnSe) Has the highest figure of merit at high temperatures of any known material. It is for this reason that researchers have investigated its structure and they discovered that another phase can exist. α -SnSe has an orthorhombic crystal structure. This means that all three sides of the unit cell have a different length. This results in a large anisotropy in the electronic structure and the thermoelectric properties[12]. The new phase has a cubic structure and is called π -SnSe or cubic-SnSe. The crystal structure of cubic SnSe is shown in figure 9.

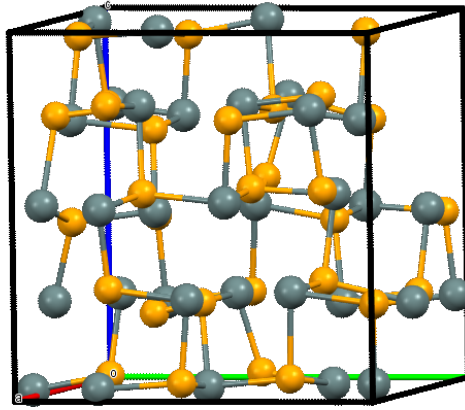


FIGURE 9: A unit cell of cubic SnSe, based on crystal information from [1]

5.2 Density of states

Since the unit cell of cubic SnSe is rather complex, it is not easy to get a good approximation of its density of states. Nevertheless, it might be possible to get a very rough estimate by using information from literature on the effective mass, band gap and the order of magnitude of the density of states. A model of the density of states on both sides of the band gap makes it possible to calculate both the Fermi-energy and the intrinsic charge carrier concentration at a given temperature. Both follow directly from charge conservation, which states that the electron and hole concentrations must be equal. These concentrations are given in equations 5 and 6. The resulting equality can be solved using Newton's method.

To confirm that this works it was tested using a symmetric density of states with the simplest structure (parabolic bands) and a band gap of 1eV. The zero of the energy scales is defined at the top of the valance band. This density of states is given in equation 23. In this case, the Fermi-energy should lie exactly in the middle of the band gap, so $\mu = 0.5eV$. The algorithm was started at $\mu = 0$, which is not a good estimate of the correct result, but it still managed to

get the correct value. When the actual model is used, starting point will be in the middle of the bandgap, since that is often a better estimate than either edge of the band gap. The test was done at a number of temperatures. The stopping condition was modified such that the algorithm stops when the difference between p_0 and n_0 relative to p_0 is smaller than 10^{-3} .

$$DOS = \begin{cases} D_{0,v} * \sqrt{-E} & \text{if } E < 0 \\ D_{0,c} * \sqrt{E - E_g} & \text{if } E > E_g \end{cases} \quad (23)$$

The results are shown in table IV. The algorithm computes the Fermi energy with the desired accuracy. It does take more iterations at lower temperatures. This is because the Fermi-Dirac function can be approximated very well with the exponential Boltzmann distribution function for energies far from the Fermi-energy. This function is given in equation 24. Away from the centre of the bandgap, one of the carrier concentrations is much lower than the other. So, only one of the concentrations is relevant and it can be approximated with 24. This is an exponential function, so, its derivative is equal to itself divided by the thermal energy. This causes the algorithm to take steps with the size of the thermal energy, until it gets close to the centre. Because the starting point is far away from the final answer, the number of iterations will increase at low temperatures. It also means that the algorithm cannot be sped up by increasing the tolerance.

$$f_B(E) = e^{-\frac{E-\mu}{k_B T}} \quad (24)$$

TABLE IV: The calculated Fermi-energy for a symmetric density of states with a band gap of 1eV.

Temperature (K)	$\mu - 0.5$ (eV)	$\frac{p_0 - n_0}{n_0}$	# Iterations
200	$-4.6 \cdot 10^{-6}$	$5.4 \cdot 10^{-4}$	31
400	$-1.4 \cdot 10^{-8}$	$7.9 \cdot 10^{-7}$	17
600	$-2.6 \cdot 10^{-7}$	$1 \cdot 10^{-5}$	12
800	$-2.1 \cdot 10^{-10}$	$6 \cdot 10^{-9}$	10
1000	$-2.4 \cdot 10^{-6}$	$5.6 \cdot 10^{-5}$	8

The band gap of π -SnSe has been measured to be 1.01eV and the effective mass was found to be $0.37m_0$. This is not a small band gap, which means that the two-band Kane model can no longer be used to find the density of states. In the analysis below a very crude model for the density of states is used, which is based on results from literature.

In [11], the Density of states of cubic SnSe was calculated. however, the resolution of their calculation near the band gap is not high enough for it to be used directly. The study can, however, be used to get the right order of magnitude. The results of their calculations are shown in figure 10.

Only the region closely around the band gap is of interest. However, due to artificial broadening of the graph, the band gap has disappeared completely. From their calculated band-structure it is clear that there should be a band gap between $E=0$ and $E=0.97\text{eV}$.

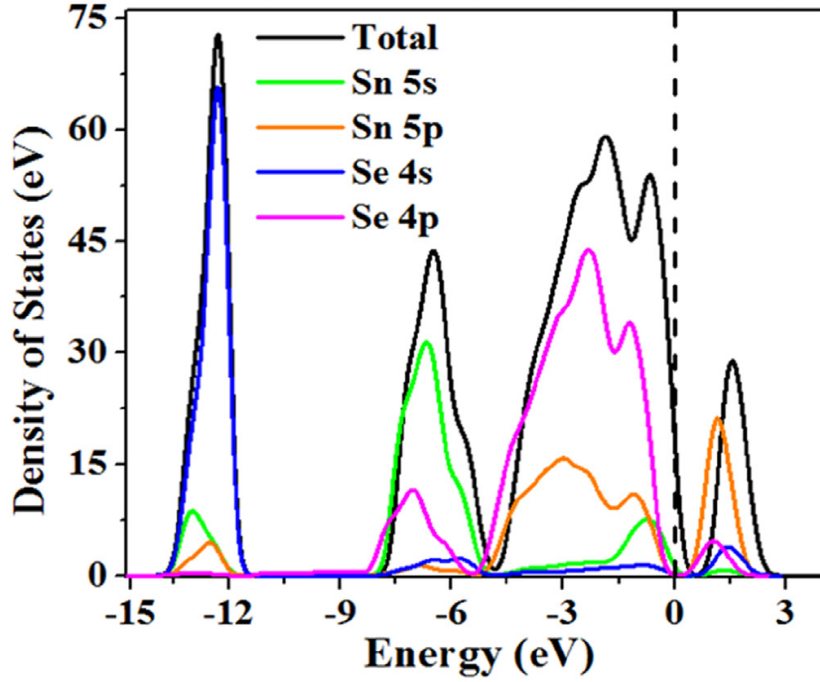


FIGURE 10: The density of states of SnSe in states per eV per electron per unit cell.

The graph will be used to get an estimate of the parameters in equation 23. The density of states at -0.5 is about 50 states per eV per electron in a unit cell a graph of the approximation can be seen in figure 11. Obviously, the approximation can only reasonably be applied for energies between -1eV and 2eV . At 900K , the thermal energy is about 0.077eV . Thus, the distance between the Fermi-energy and the edge of the region is always more than 10 times the thermal energy. The Fermi-function is then smaller than $5 * 10^{-5}$. So, If the Fermi-energy does not lie further than 0.2eV away from either edge of the bandgap, then the fact that the DOS is only approximated in a small region does not affect the results significantly. To find the total number of states, this must be multiplied by the number of electrons in the unit cell and divided by the volume of the unit cell. There are 64 atoms in the unit cell, each of which can give 1 electron. The width of a unit cell is 11.97\AA , so its volume is: $(11.97 * 10^{-10})^3 = 1.715 * 10^{-27} m^3$. [1]. This gives a final conversion factor of $3.73 * 10^{28}$.

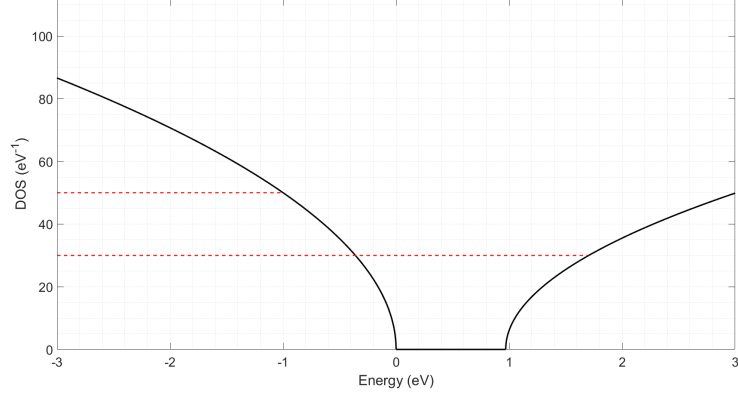


FIGURE 11: The crude model of density of states of π -SnSe in states per eV per electron per unit cell.

5.3 Thermoelectric properties

When the density of states is known, it is possible to calculate the Seebeck coefficient as a function of the Fermi-energy. This is useful, because the Fermi-energy can be changed by adding dopants to the material. Adding n-type dopants increases the Fermi-energy, while p-type dopants will decrease it. The Seebeck coefficient was calculated within the constant relaxation time approximation and the results are shown in figure 12.

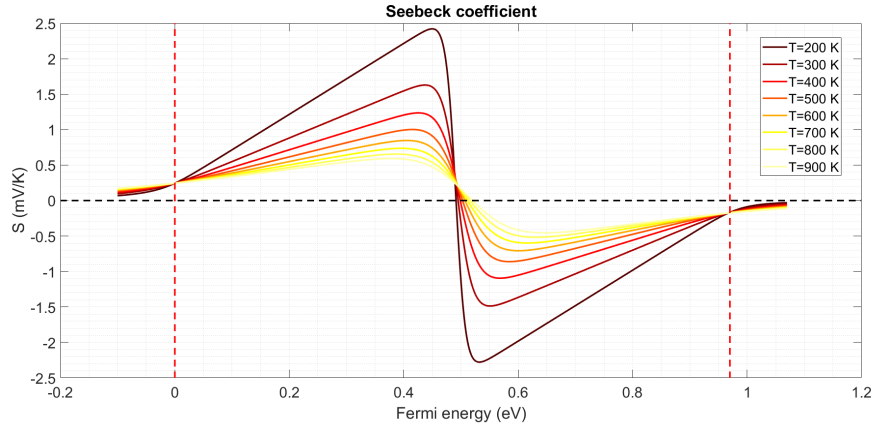


FIGURE 12: The Seebeck coefficient as a function of the Fermi-energy computed with the simple density of states. The red dotted lines mark the edges of the band gap.

A sharp transition can be seen when the Fermi energy lies in the middle of the band gap. At that point the dominant charge carrier changes from holes (low μ) to electrons (high μ). At 200K, the Seebeck coefficient increases to 2.46mV/K. This is close to the 2292mV/K that was calculated in [11]. At 900K the highest absolute value is .59mV/K, while the other article reports 0.4443mV/K. At the other temperatures the value was slightly higher than the values of the other article as well. The absolute Seebeck coefficient at the edge of the bandgap is

higher than what is found in the article. This is probably due to the very high slope of the crude model at that point. A high slope creates relatively many high energy carriers, which increases the Seebeck coefficient.

The highest Seebeck coefficient occurs near the middle of the bandgap. This is the point at which the conductivity is minimal. The electrical conductivity increases as the Fermi-energy moves away from the middle of the band gap. This is shown in figure 13. The straight lines shown that the conductivity increases exponentially with the Fermi-energy. This is to be expected in semiconductor with a large bandgap [7]. The conductivity increases monotonically with the temperature due to the increasing carrier concentration. At high temperatures the conductivity increases to the order of ($10^{19}(\Omega ms)$), which is similar to the results from [5].

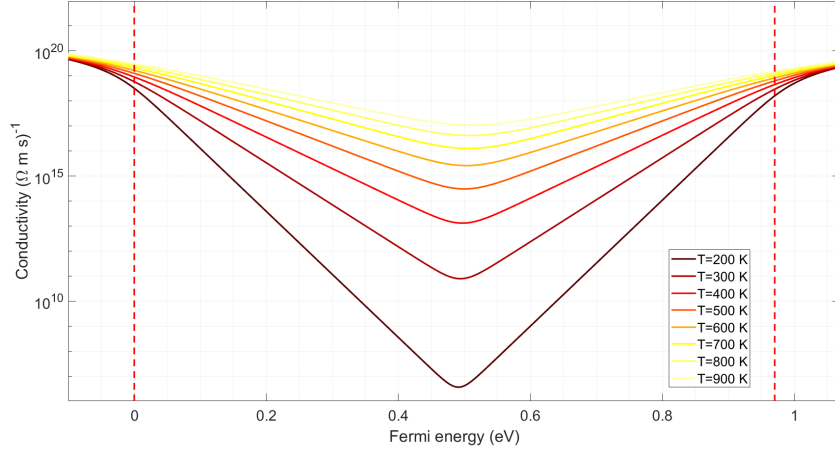


FIGURE 13: A logarithmic plot of the electrical conductivity as a function of the Fermi-energy computed with the simple density of states. The value is taken with respect to the relaxation time. The red dotted lines mark the edges of the band gap.

5.4 Power factor

The energy at which the transition occurs decreases at higher temperatures, this is due to the asymmetry in the density of states. The Seebeck coefficient is zero when the electron and hole contributions are the same. The Fermi-energy at which this happens increases with temperature, which was also found by [5]. This happens because the density of states is higher in the valence band than in the conduction band. This means that the conductivity of the holes is larger around the centre of the bandgap than the conductivity of the electrons. This means that at that point the Seebeck coefficient from the valence band is more important than the one from the conduction band. The Seebeck coefficient is not affected by the constant pre-factor in the density of states, this follows from the formula 10. This means that: $S_C(\mu) = -S_V(E_G - \mu)$ due to symmetry. This is also the reason why the Seebeck coefficient is the same when the lines cross. The asymmetry thus only comes from the conductivity. The Fermi-energy at which the two conductivities are equal increases with temperature, because the shift must compensate for the fact that the hole concentration increases faster if the Fermi-energy is kept constant. That is also the main reason for the shift of the cross-over point.

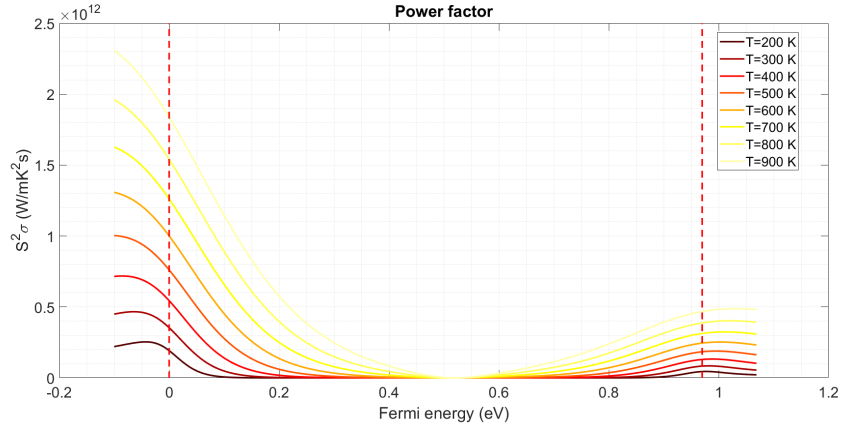


FIGURE 14: The power factor as a function of the Fermi-energy computed with the simple density of states. The value is taken with respect to the relaxation time. The red dotted lines mark the edges of the band gap.

The effect of the increase of the Conductivity and decrease of the Seebeck coefficient near the edges of the bandgap can be analysed through the power factor. The power factor of the material is plotted in figure 14. This value is again given in terms of the relaxation time. At low temperatures, the power factor reaches a local maximum when the Fermi-energy lies outside of the band gap. The power factor at the edge of the band gap is about an order of magnitude higher than what was reported in the article. The cause of this is the higher value of the Seebeck coefficient in the crude model. In figure 15 the power factor is plotted on a logarithmic scale. This shows that the position of its minimum

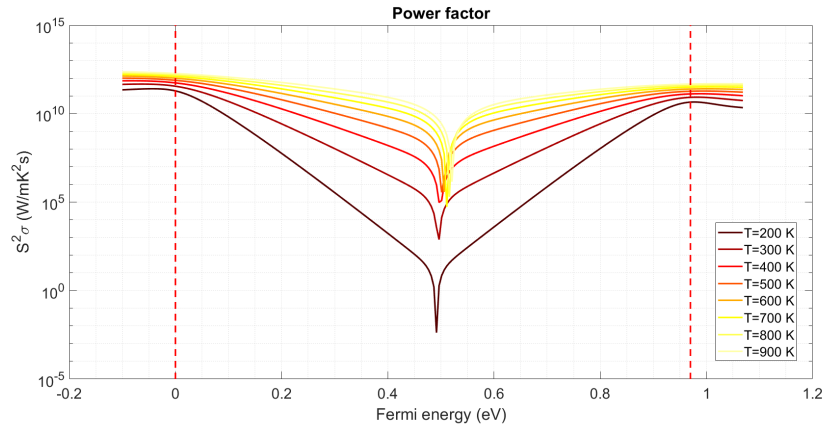


FIGURE 15: A logarithmic plot of the power factor as a function of the Fermi-energy computed with the simple density of states. The value is taken with respect to the relaxation time. The red dotted lines mark the edges of the band gap.

6 Conclusion

In this report, the thermoelectric effect has been modelled in two materials. For nanostructured PbTe a model is presented that focusses mainly on changing the material parameters of the relaxation times to improve the thermoelectric properties. The result is that at low temperatures, there is a barrier height that optimizes the Seebeck coefficient, this optimum disappears at higher temperatures. At low temperature (100K), the power factor of PbTe can be increased by adding energy barriers. The power factor of PbTe can be improved by adding energy barriers. The optimal barrier height depends on the charge carrier concentration. At 300K, adding energy barrier only decreases the power factor of PbTe.

Then π -SnSe was studied using a very crude model for the density of states. The results were similar to those found in [5]. It was found that the Seebeck coefficient is highest when the Fermi level lies between 50meV and 170meV from either side of the middle of the band gap. The exact optimum depends on the temperature. The conductivity was calculated and with it the power factor. At low temperatures, the power factor has two local maxima, one on either side of the band gap. These maxima give optimal values for the Fermi-energy that lie outside of the band gap. The carrier concentration that result from this are in the order of $10^{20}cm^{-3}$, which can only be achieved to a very large amount of doping.

7 Outlook

To get more accurate results for the properties of cubic tin selenide, a better approximation of its density of states is needed. combined with the binding energies of different impurities this would allow for the calculation of the thermoelectric properties as a function of dopant concentration and temperature alone. More information on the structural parameters of the material is needed in order to improve the model to one that does not assume a constant relaxation time

8 Acknowledgements

I would like to thank Mark Huijben and Bernard Geurts for supervising this assignment and making me enthusiastic about the topic of thermoelectricity. I would also like to thank Geert Brocks for being my second examiner from applied physics and for some valuable discussions. Finally I would like to thank Richard Boucherie for being the second examiner from the side of applied mathematics.

Bibliography

- [1] Ran E Abutbul, Elad Segev, Shmuel Samuha, Leila Zeiri, Vladimir Ezersky, Guy Makov, and Yuval Golan. A new nanocrystalline binary phase: synthesis and properties of cubic tin monoselenide. *CrystEngComm*, 18(11):1918–1923, 2016.
- [2] N.W. Ashcroft and N.D. Mermin. *Solid State Physics*. Cengage Learning, 2011.
- [3] C.M. Bhandari and D.M. Rowe. *Thermal conduction in semiconductors*. Wiley, 1988.
- [4] Kanishka Biswas, Jiaqing He, Ivan D Blum, Chun-I Wu, Timothy P Hogan, David N Seidman, Vinayak P Dravid, and Mercouri G Kanatzidis. High-performance bulk thermoelectrics with all-scale hierarchical architectures. *Nature*, 489(7416):414, 2012.
- [5] Faheem K Butt, Bakhtiar Ul Haq, Sajid ur Rehman, R Ahmed, Chuanbao Cao, and S AlFaifi. Investigation of thermoelectric properties of novel cubic phase snse: A promising material for thermoelectric applications. *Journal of Alloys and Compounds*, 715:438–444, 2017.
- [6] A F. Ioffe, L S. Stil’bans, E K. Iordanishvili, T S. Stavitskaya, A Gelbtuch, and George Vineyard. Semiconductor thermoelements and thermoelectric cooling. *Physics Today - PHYS TODAY*, 12, 01 1959.
- [7] J. R. Hook and H. E. Hall. *Solid state physics*. Wiley, 2013.
- [8] Yasuo Kanai and Katsufusa Shohno. Dielectric constant of pbte. *Japanese Journal of Applied Physics*, 2(1):6, 1963.
- [9] J Martin, Li Wang, Lidong Chen, and GS Nolas. Enhanced seebeck coefficient through energy-barrier scattering in pbte nanocomposites. *Physical review B*, 79(11):115311, 2009.
- [10] A Popescu, LM Woods, J Martin, and GS Nolas. Model of transport properties of thermoelectric nanocomposite materials. *Physical Review B*, 79(20):205302, 2009.
- [11] Sajid Ur Rehman, Faheem K Butt, Fateh Hayat, Bakhtiar Ul Haq, Zeeshan Tariq, F Aleem, and Chuanbo Li. An insight into a novel cubic phase snse for prospective applications in optoelectronics and clean energy devices. *Journal of Alloys and Compounds*, 733:22–32, 2018.
- [12] Weiran Shi, Minxuan Gao, Jinping Wei, Jianfeng Gao, Chenwei Fan, Eric Ashalley, Handong Li, and Zhiming Wang. Tin selenide (snse): growth, properties, and applications. *Advanced Science*, 5(4):1700602, 2018.
- [13] AK Sreedhar and SC Gupta. Electronic effects in elastic constants of pbte. *Physical Review B*, 5(8):3160, 1972.
- [14] Wikibooks. Calculus/newton’s method — wikibooks, the free textbook project, 2019. [Online; accessed 25-June-2019].
- [15] Wikipedia contributors. Rectangular potential barrier — Wikipedia, the free encyclopedia. https://en.wikipedia.org/w/index.php?title=Rectangular_potential_barrier&oldid=874278832, 2018. [Online; accessed 21-June-2019].

- [16] Yecheng Zhou, Wei Li, Minghui Wu, Li-Dong Zhao, Jiaqing He, Su-Huai Wei, and Li Huang. Influence of defects on the thermoelectricity in sncs: A comprehensive theoretical study. *Physical Review B*, 97(24):245202, 2018.
- [17] John M Ziman. *Principles of the Theory of Solids*. Cambridge university press, 1979.